Ultrasonics 91 (2019) 170–179

Contents lists available at ScienceDirect

Ultrasonics

journal homepage: www.elsevier.com/locate/ultras

On-line measurement of clamping force for injection molding machine using ultrasonic technology

Yao Zhao, Peng Zhao*, Jianfeng Zhang, Junye Huang, Neng Xia, Jianzhong Fu

The State Key Laboratory of Fluid Power and Mechatronic Systems, College of Mechanical Engineering, Zhejiang University, Hangzhou 310027, China
The Key Laboratory of 3D Printing Process and Equipment of Zhejiang Province, College of Mechanical Engineering, Zhejiang University, Hangzhou 310027, China

ARTICLE INFO

Keywords:
Injection molding
Clamping force
Ultrasonic technology
Sono-elasticity theory
On-line

ABSTRACT

The on-line measurement of clamping force is essential for injection molding equipment and process. A method for on-line measurement of clamping force using ultrasonic technology is proposed in this study. Based on the sono-elasticity theory, a new mathematical model is established to describe the relationship between ultrasonic propagation time and clamping force. A series of experiments are then performed to validate the proposed method. Findings show this method corresponds well with the magnetic enclosed type clamping force tester method, with difference squares less than 0.65 $(MPa)^2$, and standard deviations less than 0.11 MPa. Ultrasonic parameters influence measurement results, with larger ultrasonic probe wafer diameter and higher ultrasonic probe frequency producing better measurement accuracy. Additionally, measurement accuracy is insensitive to the sampling frequency of ultrasonic signals. The proposed method has the advantages of high accuracy and high stability, being non-interfering, non-destructive, low-cost, on-line and with good adherence to health and safety, and it has significant application prospects in injection molding production.

1. Introduction

Injection molding is the most important process for producing polymeric products. Currently, more than one third of all polymeric products are produced by the injection molding process [1–4]. The real-time measurement of clamping force is vital in this process for its influence on the life of the mold and injection molding machines as well as the quality of the final products [5–8]. Clamping force is exerted by clamping unit, causing most stress to the tie-bars. When the mold is clamped, tie-bars are subjected to an axial tensile load and stress rises to a maximum value. Clamping force is released and the tie-bar stress returns to zero [5] when the mold is opened. With cyclical mold clamping and opening, tie-bars experience cyclic alternating stress from maximum to zero. These conditions lead to frequent tie-bar break-down [9], especially in high speed injection molding machines, as shown in Fig. 1. For this reason, the on-line measurement of clamping force for injection molding machine is of great significance.

As the importance mentioned above, plenty of studies have been conducted to measure clamping force, predominantly focusing on the strain gauge method [10,11,8,12]. The strain gauge is commonly attached with magnetic force due to the complex nature and low repeatability of manual installation. Huang et al. evaluated clamping force based on a magnetic enclosed type clamping force measuring tester. They developed a searching algorithm with various clamping force settings to identify the optimum clamping force value [8]. In a study by Rao et al., a magnetic enclosed type clamping force measuring tester was used to evaluate the strain and stress of the tie-bars and their partial load rate was calculated [7]. However, this method, is not suitable in practical industrial production as the sensor is installed at the mold and product operation area and can hinder the loading and unloading of mold as well as the removal of product. The technique cannot be used over long periods of time as the mounted method is not stable and it is too expensive for large-scale industrial application. The magnetic enclosed type clamping force measuring tester technique is currently mainly used for calibrating the balance of clamping force for injection molding machine before delivery. If used in industrial production, the tie-bars would suffer unbalanced force and break down, even if calibrated. A new on-line measurement method for measuring clamping force during the injection molding process is urgently needed.

Many new measurement methods have been studied, including the ultrasound method [13–18], laser method [19–21] and magnetic suspension method [22–28]. Ultrasounds are mechanical waves with frequencies that are greater than 20 kHz [29]. Michaeli et al. combined ultrasonic technology with polymer state on-line monitoring during the injection molding process [30]. Ono et al. also contributed extensively in this area of study, inventing a high temperature ultrasonic transducer

* Corresponding author.
E-mail address: pengzhao@zju.edu.cn (P. Zhao).

https://doi.org/10.1016/j.ultras.2018.08.013
Received 20 June 2018; Received in revised form 14 August 2018; Accepted 16 August 2018
Available online 17 August 2018
0041-624X/ © 2018 Elsevier B.V. All rights reserved.

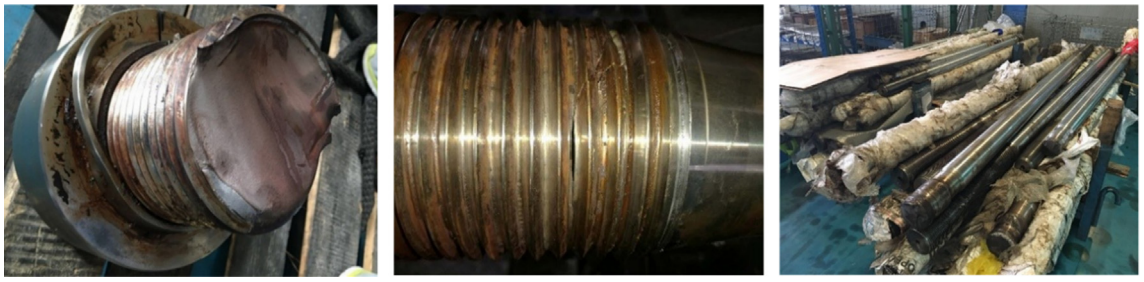

Fig. 1. Broken injection molding machine tie-bars.

used in microinjection molding [31], co-injection molding [32], and gas assisted injection molding processes [33] for on-line polymer characterization. Zhao et al. proposed an ultrasonic methodology to measure cavity pressure during the injection molding process and to calculate the degree of crystallinity for Poly(lactic acid) parts [1,34,35]. Jhang et al. established an ultrasonic velocity measurement method to estimate the clamping force in high-tension bolts [36]. No study has been undertaken on clamping force measurement for injection molding machine by ultrasonic method however.

This study proposes an on-line ultrasonic approach to measure clamping force during the injection molding process. Both experimental results and theoretical discussions are presented. Clamping force is also investigated using a magnetic enclosed type clamping force tester for comparison. Based on the sono-elasticity theory, the relationship between ultrasonic signals and clamping force is established. It is understood that this is the first attempt to measure injection clamping force via ultrasonic technology. The proposed measurement method offers the advantages of being high accuracy and high stability, non-interfering, non-destructive, on-line, low-cost and adhering to health and safety requirements.

2. Experimental methods

2.1. Mathematical model and method

During the process of injection molding, the clamping force is transmitted to the tie-bars through the mold, the moving platen and the stationary platen. As shown in Fig. 2(a), when the mold is clamped, the tie-bars are subjected to an axial tensile load and tie-bar stress rises to a maximum value. After mold opening, the clamping force is released and the tie-bar stress returns to zero, as shown in Fig. 2(b). With cyclical mold clamping and mold opening, the tie-bars experience the cyclic and alternating stress from maximum value to zero.

This study proposes a model and method for real-time non-destructive measurement of clamping force for an injection molding machine using ultrasonic technology according to the sono-elasticity theory. The sono-elasticity effect occurs when an ultrasound propagates in a tie-bar and its propagation velocity changes with the stress [37]. As the tie-bars can withstand alternating stress, the propagation velocity of the ultrasound is also varied. With the help of the propagation velocity, the stress can be obtained as [38,39]:

$$\rho_0 \cdot C_\sigma^2 = \lambda + 2\mu + \frac{\sigma}{3\lambda + 2\mu}[2l + \lambda + (\lambda + \mu)(4m + 4\lambda + 10\mu)] \tag{1}$$

where ρ_0, σ and C_σ are the density of the tie-bar, the stress of the tie-bar and the propagation velocity of ultrasound, respectively. l, m and n are the Murnaghan constants of the tie-bar, and λ and μ are the Lamé constants of the tie-bar. Assuming that $\sigma = 0$, Eq. (1) becomes:

$$\rho_0 \cdot C_0^2 = \lambda + 2\mu \tag{2}$$

Using Eq. (1) to subtract Eq. (2), produces:

$$(C_0 - C_\sigma)/C_0 = K \cdot \sigma \tag{3}$$

where
$K = [2l\mu + \lambda\mu + (\lambda + \mu)(4m + 4\lambda + 10\mu)]/[2\mu(3\lambda + 2\mu)(\lambda + 2\mu)]$ is the sono-elasticity coefficient, which is an inherent material parameter that characterizes the acoustic elastic property of the tie-bar. In this study, C_0 and C_σ are:

$$C_0 = 2l_0/t_0 \tag{4}$$

$$C_\sigma = 2l_0(1 + \sigma/E)/t_\sigma \tag{5}$$

where t_0 is the propagating time of the ultrasound in a situation where the tie-bar is subjected to no stress. Similarly to t_0, t_σ denotes the propagating time in the situation that the tie-bar stands a stress of σ. The natural length with no stress is l_0. The relative change of time $(t_\sigma - t_0)/t_0$ is set and combined with Eqs. (3)–(5), yielding:

$$(t_\sigma - t_0)/t_0 = \frac{\sigma/E + K\sigma}{1 - K\sigma} \tag{6}$$

As $K\sigma \ll 1$, the equation can be derived as:

$$\sigma = \frac{1}{K_1 \cdot t_0} \cdot (t_\sigma - t_0) \tag{7}$$

where $K_1 = \left(\frac{1}{E} + K\right)$ and is a material parameter.

As illustrated in Fig. 3, a tie-bar can be divided into two parts: l_1, the component that bears no force and l_2, the part that bears the clamping force. The propagation time through the whole tie-bar at a state of standing with no force is $t_{\text{no force}}$ and the propagation time through the

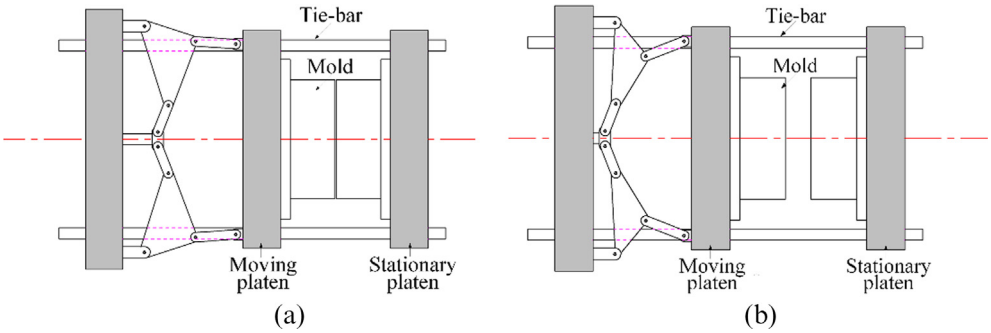

Fig. 2. Schematic diagram of tie-bars under different stress states: (a) mold clamping; (b) mold opening.

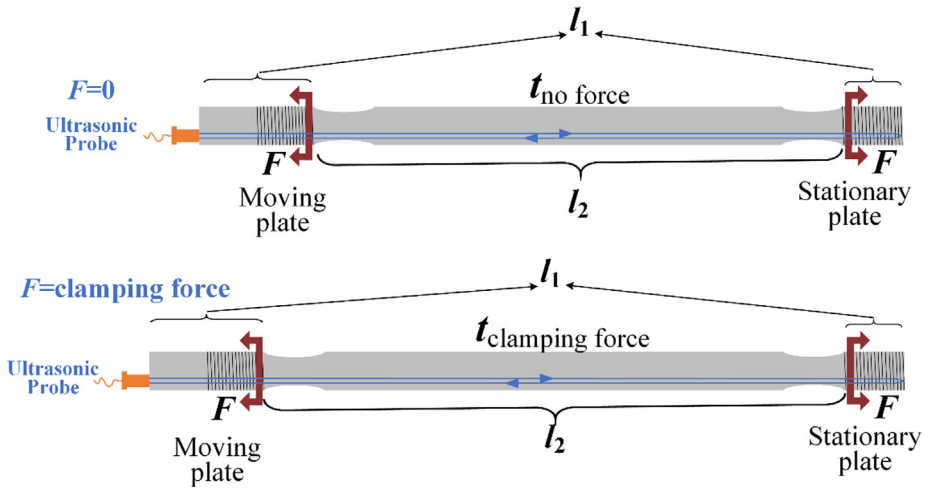

Fig. 3. Schematic diagram of actual clamping force for tie-bars in industrial production.

whole tie-bar at a state of standing a clamping force is $t_{\text{clamping force}}$.

$$t_0 = l_2/(l_1 + l_2)\cdot t_{\text{noforce}} \tag{8}$$

$$t_\sigma = t_{\text{clampingforce}} - l_1/(l_1 + l_2)\cdot t_{\text{noforce}} \tag{9}$$

In combining Eqs. (7)–(9), the clamping stress σ in a tie-bar can be calculated, as demonstrated in Eq. (10):

$$\sigma = F/S = \frac{1}{K_1\cdot l_2/(l_1 + l_2)\cdot t_{\text{noforce}}}\cdot(t_{\text{clampingforce}} - t_{\text{noforce}}) \tag{10}$$

where F is the clamping force and S denotes the cross-sectional area of the tie-bar. Notably, materials properties include modulus of elasticity (E), Murnaghan constants (l, m, n) and Lamé constants (λ and μ) were integrated into one parameter K_1, i.e., $K_1 = \frac{1}{E} + K = \frac{1}{E} + [2l\mu + \lambda\mu + (\lambda + \mu)(4m + 4\lambda + 10\mu)]$. The value of K_1 can be determined by a calibration method. Through measuring ultrasonic propagation time under known clamping force and Eq. (10), the parameter K_1 can be obtained.

2.2. Measurement device

The clamping force measurement device is shown in Fig. 4. The ultrasonic signal probes are four longitudinal wave pulsing/receiving ultrasonic transducers (Shantou Institute of Ultrasonic Instruments Co., Ltd., China) with the same specifications. The four tie-bars have been numbered from #1 to #4 for easy identification. An ultrasonic signal transmitter receiver (CTS-8077PR, Shantou Institute of Ultrasonic Instruments Co., Ltd., China) and a digital oscilloscope (InfiniiVision DSO-X-2002A, Agilent Technologies Co., Ltd., America) were combined to collect, process and display the ultrasonic signals. The equipment to be studied was an injection molding machine (HAITIAN380, Haitian International Holdings Co., Ltd., China). As shown in Fig. 4, the ultrasonic probes were strongly mounted on the bottom of the tie-bars with the aid of glue, avoiding the central positioning hole. The machine vibration can hardly interfere the ultrasonic measurement results.

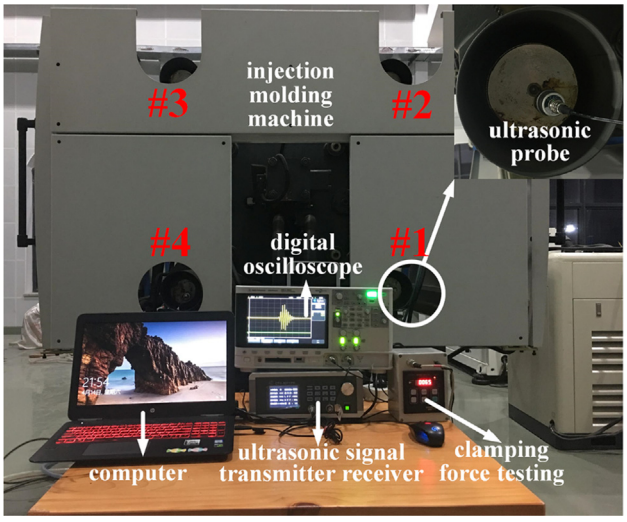

Fig. 4. Diagram of the measurement system and the emphases display of the ultrasonic probe.

2.3. Verification device and method

A magnetic enclosed type clamping force tester (Monitor DU-1D, GEFRAN Sensors Co., Ltd., Italy) was attached to the outside surface of the tie-bars to verify the accuracy of the proposed ultrasonic method. The magnetic enclosed type clamping force tester will be subsequently referred to here as the clamping force tester. This tester was directly fixed on the flat part of the tie-bar, close to the side of the stationary platen so as not to hinder the mold clamping.

The difference square, $\bar{\delta}$, was used to specifically measure the deviation of the ultrasonic measurement results corresponding to the clamping force tester results. The equation is as follows:

$$\bar{\delta} = \frac{1}{n}\cdot\sum_{i=1}^{n}(\sigma_i - \sigma_j)^2 \tag{11}$$

where σ_i is the clamping stress with clamping force tester; σ_j is the clamping force with ultrasonic method, and n is the experiment times, $n = 3$. The standard deviation, s, was employed to specifically measure the stability of the measurement results, as shown in Eq. (12):

$$s = \frac{1}{n}\cdot\sqrt[2]{\sum_{i=1}^{n}(\sigma_j - \bar{\sigma})^2} \tag{12}$$

where $\bar{\sigma}$ is the average clamping stress under certain clamping force. The standard deviation of clamping stress for the clamping force tester is s_i, and the standard deviation of the clamping stress for the ultrasonic method is s_j.

3. Results and discussion

According to the model and method, a series of experiments were conducted. The injection molding machine used in the study was HAITIAN 380. The l_1, l_2 were 400 mm, and 3010 mm, respectively. The

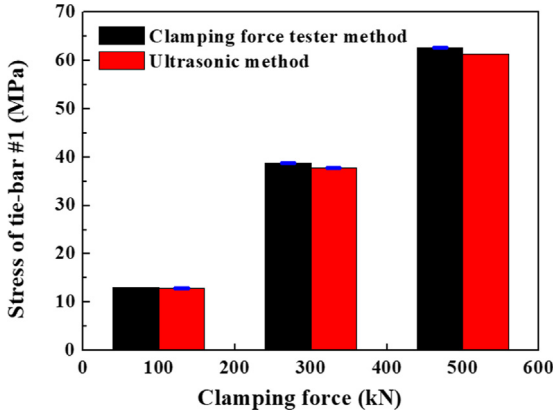

Fig. 5. The measured stresses as well as the error bar of #1 tie-bar under two methods.

Table 1
Comparison results for #1 tie-bar under two methods.

F (kN)	$t_{noforce}$ (ns)	$t_{clampingforce}$ (ns)	σ_i (MPa)	s_i (MPa)	σ_j (MPa)	s_j (MPa)	$\bar{\delta}$ $(MPa)^2$
~100	1,159,020	1,159,238	13.114	0	12.792	0.040	0.055
	1,159,025	1,159,245	13.114		12.939		
	1,159,015	1,159,235	13.114		12.939		
~300	1,159,015	1,159,660	38.834	0.035	37.934	0.080	1.124
	1,159,025	1,159,665	38.706		37.640		
	1,159,020	1,159,660	38.834		37.640		
~500	1,159,020	1,160,060	62.771	0.035	61.165	0	2.318
	1,159,020	1,160,060	62.643		61.165		
	1,159,020	1,160,060	62.643		61.165		

material parameter K_1 was 1.662×10^{-11}. The diameter of the tie-bar was 100 mm.

3.1. Preliminary verification experiments

A set of experiments for preliminary verification were initially conducted. A commonly used ultrasonic probe (5P6) [29,34,35] with a wafer diameter of 6 mm and a frequency of 5 MHz was studied in this section. The sampling frequency of the echo signals were 100 MHz and the #1 tie-bar was used. The clamping forces of the measured tie-bar were about 100 kN, 300 kN and 500 kN. Each experiment was conducted three times to avoid accidental errors. The stresses of tie-bars under two methods are shown in Fig. 5 and the specific data analyzed from the two methods are displayed in Table 1.

Two conclusions can be drawn from results seen in Fig. 5 and Table 1: first, the ultrasonic method was preliminarily proven to be correct. As shown in Table 1, the difference square, $\bar{\delta}$, were 0.055 $(MPa)^2$, 1.124 $(MPa)^2$ and 2.318 $(MPa)^2$ with clamping force increasing from 100 kN to 500 kN. This accuracy is acceptable in industrial production. Secondly, the ultrasonic method has excellent stability. As illustrated in Fig. 5, the error bars of the ultrasonic measurement results were relatively small and were as good as the clamping force tester method. The standard deviation, s_j, were 0.040 MPa, 0.080 MPa and 0 MPa with clamping force increasing from 100 kN to 500 kN.

3.2. Ultrasonic parameters optimization experiments

For further study of the proposed method, a set of experiments were performed with the aim of optimizing the ultrasonic measurement parameters. In this section, three process parameters, including the probe wafer diameter, ultrasonic probe frequency and sampling frequency of echo signals were selected to be investigated. To find the

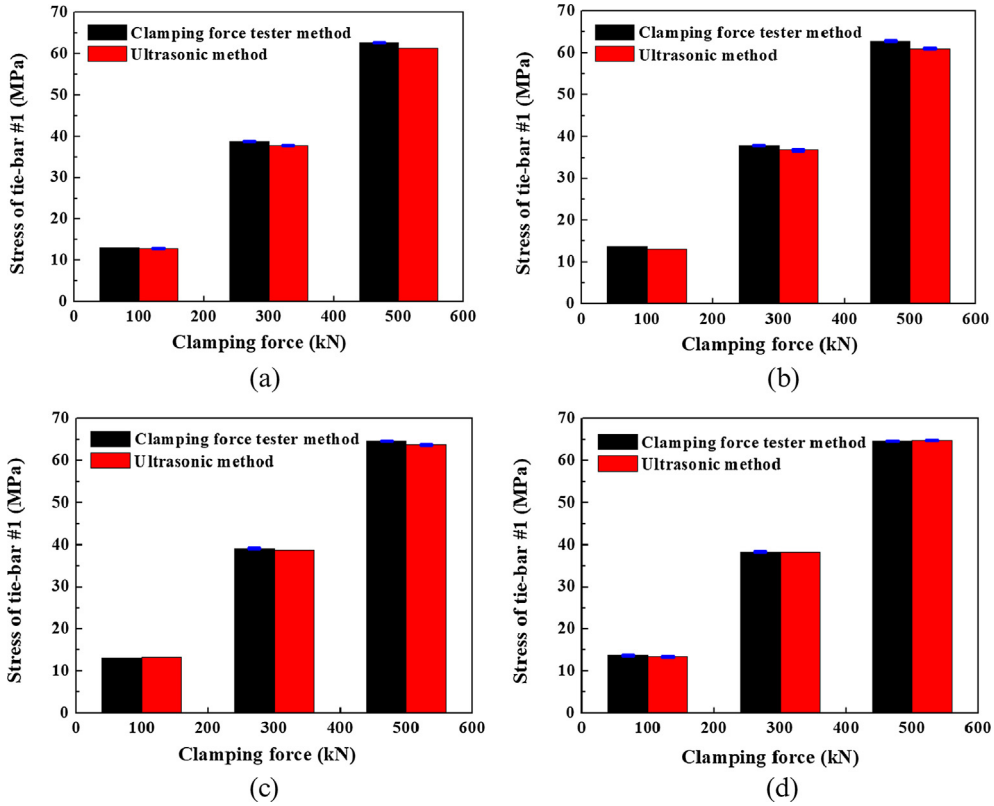

Fig. 6. Tie-bar stress measurement results of two methods under different clamping force (100 kN, 300 kN, 500 kN) and different probe wafer diameters (6 mm, 10 mm, 14 mm, 20 mm): (a) 5P6; (b) 5P10; (c) 5P14; (d) 5P20.

Table 2
Comparison results for #1 tie-bar with two methods under different clamping force and different probe wafer diameters.

Probe	F	$t_{noforce}$	$t_{clampingforce}$	σ_i	s_i	σ_j	s_j	$\bar{\delta}$
	(kN)	(ns)	(ns)	(MPa)	(MPa)	(MPa)	(MPa)	$(MPa)^2$
5P6	~100	1,159,020	1,159,238	13.114	0	12.792	0.040	0.055
		1,159,025	1,159,245	13.114		12.939		
		1,159,015	1,159,235	13.114		12.939		
	~300	1,159,015	1,159,660	38.834	0.035	37.960	0.080	1.072
		1,159,025	1,159,665	38.706		37.665		
		1,159,020	1,159,660	38.834		37.665		
	~500	1,159,020	1,160,060	62.771	0.035	61.246	0	2.077
		1,159,020	1,160,060	62.643		61.246		
		1,159,020	1,160,060	62.643		61.246		
5P10	~100	1,159,018	1,159,233	13.751	0	13.150	0	0.361
		1,159,023	1,159,238	13.751		13.150		
		1,159,023	1,159,238	13.751		13.150		
	~300	1,159,018	1,159,616	37.688	0.035	36.546	0.042	1.176
		1,159,018	1,159,618	37.688		36.699		
		1,159,018	1,159,618	37.815		36.699		
	~500	1,159,028	1,160,023	62.771	0.035	60.858	0.0001	3.342
		1,159,023	1,160,018	62.643		60.859		
		1,159,018	1,160,013	62.643		60.859		
5P14	~100	1,158,975	1,159,200	13.114	0	13.233	0	0.014
		1,158,970	1,159,195	13.114		13.233		
		1,158,975	1,159,200	13.114		13.233		
	~300	1,158,965	1,159,625	39.216	0.035	38.818	0	0.130
		1,158,960	1,159,620	39.088		38.818		
		1,158,965	1,159,625	39.216		38.818		
	~500	1,158,950	1,160,030	64.681	0.035	63.521	0.080	0.880
		1,158,950	1,160,035	64.681		63.815		
		1,158,950	1,160,035	64.553		63.815		
5P20	~100	1,159,145	1,159,370	13.623	0.035	13.231	0.080	0.144
		1,159,145	1,159,370	13.751		13.231		
		1,159,150	1,159,380	13.624		13.525		
	~300	1,159,150	1,159,800	38.324	0.060	38.224	0	0.021
		1,159,150	1,159,800	38.197		38.224		
		1,159,155	1,159,805	38.452		38.224		
	~500	1,159,160	1,160,260	64.681	0.035	64.686	0.0001	0.012
		1,159,170	1,160,270	64.553		64.685		
		1,159,160	1,160,260	64.553		64.686		

optimum parameter, one of the three process parameters mentioned above was changed, while the other two remained the same.

3.2.1. Influences of ultrasonic probe wafer diameter

The frequency of the ultrasonic probe and sampling frequency of echo signals were maintained at 100 MHz. Probes with wafer diameters of 6 mm, 10 mm, 14 mm and 20 mm were mounted on the #1 tie-bar to measure clamping force. The clamping forces of the measured tie-bars were set as about 100 kN, 300 kN, 500 kN, and each experiment was performed three times to avoid accidental error. Meanwhile, the clamping force tester was used to evaluate the effect of each measurement under different process parameters.

The measured stresses of the tie-bar under two methods are shown in Fig. 6. Probe wafer diameter differed from 6 mm, 10 mm, 14 mm and 20 mm. The specific data analyzed from the two methods is illustrated in Table 2.

Results in Fig. 6 and Table 2 clearly indicate that the wafer diameter of the ultrasonic probe is generally positively correlated with measurement accuracy. A larger probe wafer diameter induces higher measurement accuracy, as long as the probe wafer diameter is less than the measured tie-bar radius. Specifically, when the wafer diameter of the probe is relatively small (such as 6 mm or 10 mm), the difference square values, $\bar{\delta}$, are greater than 1 $(MPa)^2$. Therefore, small wafer diameters should be avoided as far as possible. On the basis of previous studies, for slender rods, such as injection molding machine tie-bars, the propagation and the measurement effect of ultrasonic waves is determined by the directivity of the ultrasonic signals, and the directivity of the ultrasonic wave is related to the diffusion angle. The smaller the diffusion angle, the better the directivity. The semi-diffusion angle θ_0 of the ultrasonic has a quantitative relationship with the probe wafer diameter D_s and the ultrasonic wavelength λ.

$$\theta_0 = \arcsin 1.22\frac{\lambda}{D_s} \approx 70\frac{\lambda}{D_s} \tag{13}$$

According to Eq. (13), the larger the wafer diameter of the probe, the better the directivity and the smaller the error. Based on the experiment and theory, a large ultrasonic probe diameter will produce higher accuracy. With this in mind, the ultrasonic probe with a wafer diameter of 20 mm was selected.

3.2.2. Influences of ultrasonic probe frequency

With probe wafer diameter of 20 mm selected, a set of experiments intended to optimize the frequency of ultrasound was then performed. Frequencies were 1 MHz, 2.5 MHz and 5 MHz. The probe wafer diameter and the sampling frequency of echo signals were maintained 20 mm, 100 MHz, respectively. The clamping forces were set as about 100 kN, 300 kN, 500 kN, and each experiment was done three times to avoid accidental error. The stresses of tie-bars under two methods are shown in Fig. 7 and specific data analyzed from the two methods are clarified in Table 3.

As seen in Fig. 7 and Table 3, measurement accuracy is insensitive to the ultrasonic probe frequency. The $\bar{\delta}$ under frequency of 1 MHz, 2.5 MHz and 5 MHz was 0.091 $(MPa)^2$, 0.105 $(MPa)^2$ and 0.059 $(MPa)^2$, respectively. The wavelength, λ, and semi-diffusion angle of the

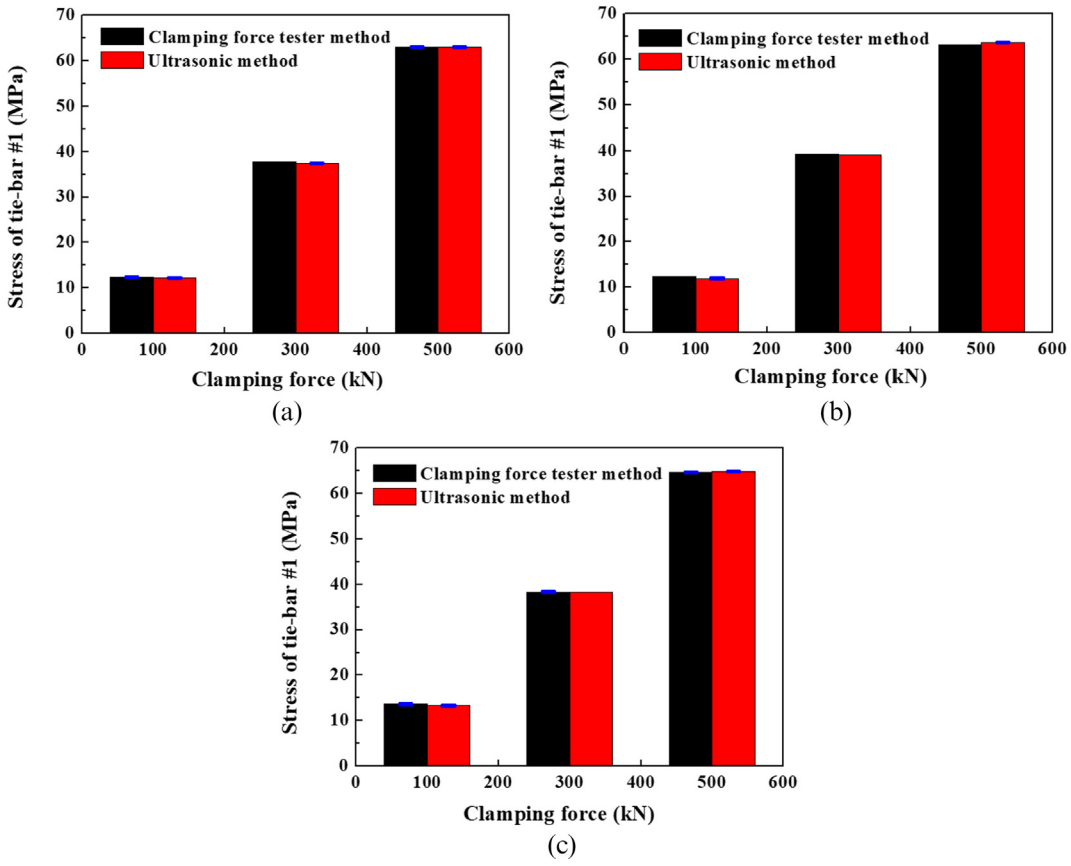

Fig. 7. Tie-bar stress measurement results of two methods under different clamping force (100 kN, 300 kN, 500 kN) and different ultrasonic probe frequency (1 MHz, 2.5 MHz, 5 MHz): (a) 1P20; (b) 2.5P20; (c) 5P20.

Table 3
Comparison results for #1 tie-bar with two methods under different clamping force and different ultrasonic frequency.

Probe	F	$t_{noforce}$	$t_{clampingforce}$	σ_i	s_i	σ_j	s_j	$\bar{\delta}$
	(kN)	(ns)	(ns)	(MPa)	(MPa)	(MPa)	(MPa)	$(MPa)^2$
1P20	~100	1,159,110	1,159,318	12.478	0.035	12.203	0.040	0.038
		1,159,110	1,159,320	12.478		12.350		
		1,159,115	1,159,323	12.350		12.203		
	~300	1,159,105	1,159,740	37.815	0	37.343	0.0004	0.223
		1,159,120	1,159,755	37.815		37.343		
		1,159,070	1,159,705	37.815		37.344		
	~500	1,159,095	1,160,163	62.898	0.035	62.778	0.040	0.012
		1,159,080	1,160,150	63.025		62.926		
		1,159,115	1,160,185	63.025		62.924		
2.5P20	~100	1,159,110	1,159,310	12.350	0	11.762	0.080	0.174
		1,159,095	1,159,300	12.350		12.056		
		1,159,100	1,159,305	12.350		12.056		
	~300	1,159,115	1,159,780	39.216	0	39.107	0	0.011
		1,159,115	1,159,780	39.216		39.107		
		1,159,115	1,159,780	39.216		39.107		
	~500	1,159,055	1,160,135	63.153	0	63.515	0.0001	0.131
		1,159,060	1,160,140	63.153		63.515		
		1,159,065	1,160,145	63.153		63.515		
5P20	~100	1,159,145	1,159,370	13.624	0.035	13.231	0.080	0.145
		1,159,145	1,159,370	13.751		13.231		
		1,159,150	1,159,380	13.624		13.525		
	~300	1,159,150	1,159,800	38.324	0.060	38.224	0	0.021
		1,159,150	1,159,800	38.197		38.224		
		1,159,155	1,159,805	38.452		38.224		
	~500	1,159,160	1,160,260	64.681	0.035	64.686	0.0001	0.012
		1,159,170	1,160,270	64.553		64.685		
		1,159,160	1,160,260	64.553		64.686		

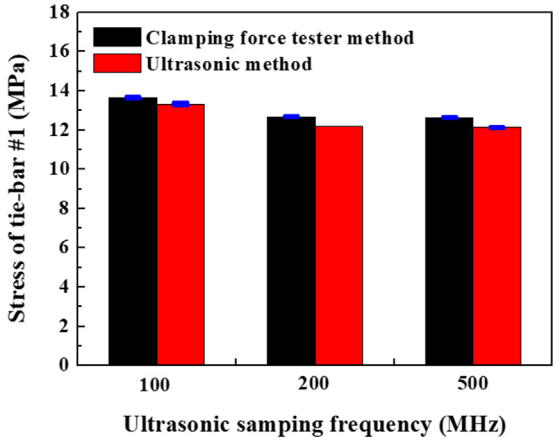

Fig. 8. Tie-bar stress measurement results of two methods under different sampling frequency of echo signals sampling (100 MHz, 200 MHz, 500 MHz).

ultrasonic, θ_0, will decrease with the increasing of ultrasonic probe frequency, which can not only enhance the directivity, but also help improve the resolution. Therefore, it is appropriate to choose 5 MHz as the optimal frequency.

3.2.3. Influences of ultrasonic sampling frequency

A set of experiments aimed to optimize the ultrasonic sampling frequency were carried out. The sampling frequencies of echo signals were 100 MHz, 200 MHz and 500 MHz. The probe wafer diameter was maintained at 20 mm and ultrasonic probe frequency was 5 MHz. The clamping force of the measured tie-bar was set to about 100 kN, and each experiment was carried out three times. The stresses of tie-bars under two methods are shown in Fig. 8 and specific data analyzed from the two methods are displayed in Table 4. It is important to note that the studied equipment is a toggle injection molding machine, and its clamping force cannot be precisely controlled at a certain value. Hence, in Table 4, the clamping force can only be roughly adjusted to around 100 kN, and the actual clamping force will vary over different experiments groups.

The measurement accuracy was found to be insensitive to the sampling frequency of echo signals, as the $\bar{\delta}$ is less than 0.27 $(MPa)^2$ in all three measured sampling frequencies. Theoretically, the higher the ultrasonic sampling frequency is, the higher the measurement accuracy is. However, in this study, the sampling frequency is sufficiently high that the difference in measurement accuracy is not obvious. Moreover, considering the cost of data acquisition equipment is directly related to the ultrasonic sampling frequency, choosing a smaller sampling frequency can reduce the cost of equipment. Due to this, 100 MHz was selected as the optimal frequency.

In summary, the optimum ultrasonic measurement parameters found were: probe wafer diameter at 20 mm; ultrasonic probe frequency of 5 MHz and sampling frequency of echo signals at 100 MHz.

3.3. Verification experiments with optimized ultrasonic parameters

Using the optimized experimental parameters, the other two tie-bars of the injection molding machine were measured. The clamping forces of the injection molding machine were set as about 100 kN, 200 kN, 300 kN, 400 kN and 500 kN, respectively, and the stresses of tie-bars #2 and #4 were measured under each clamping force. To avoid accidental errors, each experiment was repeated five times. Results are shown as Fig. 9 and Table 5.

Fig. 9 and Table 5 show the measurement results with optimized ultrasonic parameters are accurate. The $\bar{\delta}$ of the two tie-bars was less than 0.65 $(MPa)^2$ and the s_j was less than 0.11 MPa under all clamping forces, proving that the optimized ultrasonic method corresponds well with the clamping force tester method. In short, the new ultrasonic method of real-time nondestructive testing for clamping force of injection molding machines is feasible with high accuracy and stability. Moreover, in this study, materials properties were integrated into one parameter K_1, and it is a temperature-dependent parameter. The impact of material parameter K_1 on the calculated stress was calculated by error analysis. The uncertainty of calculated stress was calculated, as shown in Eq. (14).

$$\delta\sigma = \left|\frac{\partial\sigma}{\partial K_1}\right|\cdot\delta K_1 = \left|\frac{t_{\text{clampingforce}} - t_{\text{noforce}}}{K_1^2\cdot l_2/(l_1+l_2)\cdot t_{\text{noforce}}}\right|\cdot\delta K_1 \tag{14}$$

where $\delta\sigma$ and δK_1 are the uncertainty of calculated stress and K_1, respectively. We define that $t_{\text{noforce}} = 1159020$ ns, $t_{\text{clampingforce}} = 1159237.5$ ns, $l_1 = 400$ mm, $l_2 = 3010$ mm, $K_1 = 1.662 \times 10^{-11}$. Using Eq. (14), $\delta\sigma = 1.262 \times 10^{12}\,\delta K_1$. Assuming that $\delta K_1 = 1 \times 10^{-12}$, a typical result of the uncertainty of the calculated stress is $\delta\sigma = 1.262$ Mpa. Hence, the proposed ultrasonic measurement method should be better performed in a production environment with a uniform temperature.

3.4. Advantages of the proposed method

Compared with other clamping force measurement methods, this technique for on-line measurement of clamping force for an injection molding machine is a potentially powerful technology. The advantages of the proposed method are:

(1) High accuracy and high stability. The difference square between the ultrasonic method and the clamping force tester method was less than 0.65 $(MPa)^2$, displaying excellent accuracy. The standard deviation of the optimized ultrasonic method was less than 0.11 MPa, also demonstrating very high stability.
(2) Non-interfering. The magnetic enclosed type clamping force tester is attached to the outside surface of tie-bars, which is a hindrance in industrial production as it is installed at the mold and product

Table 4
Comparison results for #1 tie-bar with two methods under different clamping force and different sampling frequency.

Sampling frequency (MHz)	F (kN)	t_{noforce} (ns)	$t_{\text{clampingforce}}$ (ns)	σ_i (MPa)	s_i (MPa)	σ_j (MPa)	s_j (MPa)	$\bar{\delta}$ $(MPa)^2$
100	~100	1,159,145	1,159,370	13.624	0.035	13.231	0.080	0.145
		1,159,145	1,159,370	13.751		13.231		
		1,159,150	1,159,380	13.624		13.525		
200	~100	1,158,913	1,159,121	12.732	0.035	12.205	0	0.239
		1,158,915	1,159,123	12.732		12.205		
		1,158,913	1,159,121	12.605		12.205		
500	~100	1,158,917	1,159,955	12.732	0.035	12.205	0.029	0.262
		1,158,915	1,159,943	12.605		12.087		
		1,158,916	1,159,946	12.605		12.116		

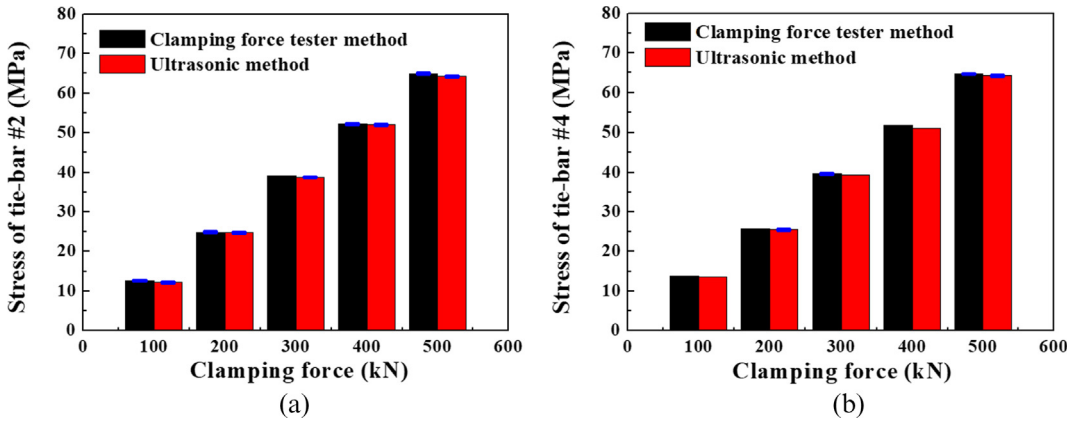

Fig. 9. #2 and #4 tie-bar stress measurement results of the injection molding machine: (a) #2 tie-bar; (b) #4 tie-bar.

Table 5
Comparison results for #2 and #4 tie-bars under two methods.

Tie-bar No.	F	t_0	$t_{clampingforce}$	σ_i	s_i	σ_j	s_j	$\bar{\delta}$
	(kN)	(ns)	(ns)	(MPa)	(MPa)	(MPa)	(MPa)	$(MPa)^2$
2	~100	1,158,965	1,159,175	12.605	0.012	12.351	0.064	0.181
		1,158,965	1,159,175	12.605		12.351		
		1,158,965	1,159,170	12.605		12.057		
		1,158,965	1,159,170	12.605		12.057		
		1,158,965	1,159,170	12.478		12.057		
	~200	1,158,960	1,159,385	25.083	0.040	24.996	0.053	0.033
		1,158,965	1,159,385	24.956		24.702		
		1,158,965	1,159,385	24.956		24.702		
		1,158,970	1,159,390	24.828		24.702		
		1,158,965	1,159,385	24.828		24.702		
	~300	1,158,960	1,159,620	39.088	0	38.818	0.0001	0.073
		1,158,960	1,159,620	39.088		38.818		
		1,158,955	1,159,615	39.088		38.818		
		1,158,935	1,159,595	39.088		38.819		
		1,158,955	1,159,615	39.088		38.818		
	~400	1,158,895	1,159,780	52.203	0.040	52.054	0.052	0.089
		1,158,895	1,159,780	52.076		52.054		
		1,158,905	1,159,790	52.330		52.054		
		1,158,910	1,159,795	52.203		52.054		
		1,158,885	1,159,765	52.330		51.761		
	~500	1,158,890	1,159,975	65.063	0.026	63.818	0.105	0.643
		1,158,860	1,159,955	65.063		64.408		
		1,158,905	1,160,000	64.935		64.406		
		1,158,900	1,159,995	64.935		64.406		
		1,158,905	1,159,995	64.935		64.112		
4	~100	1,159,010	1,159,240	13.878	0	13.527	0	0.124
		1,159,025	1,159,255	13.878		13.527		
		1,159,020	1,159,250	13.878		13.527		
		1,159,025	1,159,255	13.878		13.527		
		1,159,020	1,159,250	13.878		13.527		
	~200	1,159,000	1,159,435	25.847	0	25.584	0.053	0.117
		1,159,000	1,159,435	25.847		25.584		
		1,159,000	1,159,430	25.847		25.290		
		1,159,000	1,159,435	25.847		25.583		
		1,159,005	1,159,440	25.847		25.584		
	~300	1,159,000	1,159,670	39.598	0.022	39.405	0	0.050
		1,158,995	1,159,665	39.725		39.405		
		1,158,995	1,159,665	39.598		39.405		
		1,159,000	1,159,670	39.598		39.405		
		1,159,000	1,159,670	39.598		39.405		
	~400	1,158,900	1,159,770	51.821	0	51.172	0	0.421
		1,158,910	1,159,780	51.821		51.172		
		1,158,910	1,159,780	51.821		51.172		
		1,158,905	1,159,775	51.821		51.172		
		1,158,905	1,159,775	51.821		51.172		
	~500	1,158,915	1,160,010	64.681	0.026	64.405	0.053	0.371
		1,158,910	1,160,000	64.808		64.111		
		1,158,905	1,159,995	64.808		64.112		
		1,158,910	1,160,000	64.681		64.111		
		1,158,905	1,159,995	64.808		64.112		

operation area. The ultrasonic probes are instead mounted on the bottom of the tie-bars with the aid of glue, not interfering with the injection molding production.

(3) On-line. With the ultrasonic method, the clamping force of the whole injection process can be measured on-line. As the velocity of ultrasonic propagation is high, real-time ultrasonic signals can be gathered.

(4) Non-destructive. Ultrasonic probes are installed on the bottom of the tie-bars meaning this method does not destroy the machine or the mold.

(5) Low-cost. The total cost of the required ultrasonic equipment was much cheaper than the magnetic enclosed type clamping force tester equipment. With rapid development of transducer materials, microprocessors and signal processing methods, ultrasonic technology can be executed more economically.

(6) Health and safety. Ultrasounds are mechanical waves, and the proposed monitoring method is environmental friendly.

4. Conclusions

A model and method for online measuring of the clamping force of the injection molding machine via ultrasonic technology was proposed, and the effects of ultrasonic probe wafer diameter, ultrasonic probe frequency and ultrasonic sampling frequency were studied. Based on the results obtained in this study, the following conclusions can be drawn. First, according to the established mathematical model and method, the clamping force of the injection molding machine can be measured via ultrasonic technology. Experimental results show the proposed ultrasonic method agrees well with the magnetic enclosed type clamping force tester method, and the difference squares are less than 0.65 $(MPa)^2$ with standard deviations less than 0.11 MPa. Secondly, it was found that ultrasonic parameters influence measurement results. Larger ultrasonic probe wafer diameters and higher ultrasonic probe frequency induced better measurement accuracy. Additionally, measurement accuracy was insensitive to the sampling frequency of ultrasonic signals. The optimum ultrasonic measurement parameters discovered in this study were probe wafer diameter of 20 mm, ultrasonic probe frequency at 5 MHz, and a sampling frequency of echo signals at 100 MHz. Finally, the ultrasonic method for measuring the clamping force of an injection molding machine has the advantages of being high accuracy and high stability, non-interfering, on-line, non-destructive, low-cost and health and safety conscious. It is understood that this study is the first attempt to employ ultrasonic technology for measurement of clamping force. Using an on-line clamping force measurement method employing ultrasonic technology can greatly protect injection molding equipment and improve injection molding production efficiency.

Acknowledgements

The authors would like to acknowledge the financial support of the Zhejiang Provincial Natural Science Foundation of China (No. LZ18E050002), the Science Fund for Creative Research Groups of the National Natural Science Foundation of China (No. 51521064), the National Natural Science Foundation Council of China (No. 51475420 & No. 51635006), and the Fundamental Research Funds for the Central Universities of China (No. 2017QNA4003).

References

[1] P. Zhao, H.M. Zhou, Y. He, K. Cai, J.Z. Fu, A nondestructive online method for monitoring the injection molding process by collecting and analyzing machine running data, Int. J. Adv. Manuf. Technol. 72 (5–8) (2014) 765–777, https://doi.org/10.1007/s00170-014-5711-0.

[2] F. Bai, H.F. Zheng, Y.B. Wang, C. Wang, S.A. Liao, Research on machine vision system of monitoring injection molding processing, in: Seventh International Symposium on Precision Mechanical Measurements, vol. 9903, 2016. https://doi.org/10.1117/12.22113103.

[3] P. Zhao, H.M. Zhou, Y. Li, D.Q. Li, Process parameters optimization of injection molding using a fast strip analysis as a surrogate model, Int. J. Adv. Manuf. Technol. 49 (9–12) (2010) 949–959, https://doi.org/10.1007/s00170-009-2435-7.

[4] S. Kitayama, M. Yokoyama, M. Takano, S. Aiba, Multi-objective optimization of variable packing pressure profile and process parameters in plastic injection molding for minimizing warpage and cycle time, Int. J. Adv. Manuf. Technol. 92 (9–12) (2017) 3991–3999, https://doi.org/10.1007/s00170-017-0456-1.

[5] M.S. Huang, S.C. Nian, J.Y. Chen, C.Y. Lin, Influence of clamping force on tie-bar elongation, mold separation, and part dimensions in injection molding, Precis. Eng.-J. Int. Soc. Precis. Eng. Nanotechnol. 51 (2018) 647–658, https://doi.org/10.1016/j.precisioneng.2017.11.007.

[6] M.H. Chiang, F.L. Yang, Y.N. Chen, Y.P. Yeh, Integrated control of clamping force and energy-saving in hydraulic injection moulding machines using decoupling fuzzy sliding-mode control, Int. J. Adv. Manuf. Technol. 27 (1–2) (2005) 53–62, https://doi.org/10.1007/s00170-004-2138-z.

[7] B.Q. Rao, H.W. Zhou, H.B. Ouyang, Y.J. Wan, Y.H. Zhang, J.Y. Wu, Study on the clamping force measurement and partial load regulation technology of injection molding machine, CIRP J. Manuf. Sci. Technol. 19 (2017) 19–24, https://doi.org/10.1016/j.cirpj.2017.03.001.

[8] M.S. Huang, C.Y. Lin, A novel clamping force searching method based on sensing tie-bar elongation for injection molding, Int. J. Heat Mass Transf. 109 (2017) 223–230, https://doi.org/10.1016/j.ijheatmasstransfer.2017.02.004.

[9] C. Sasikumar, S. Srikanth, S.K. Das, Analysis of premature failure of a tie bar in an injection molding machine, Eng. Fail. Anal. 13 (8) (2006) 1246–1259, https://doi.org/10.1016/j.engfailanal.2005.11.003.

[10] Y. Zhang, T. Mao, Z.G. Huang, H. Gao, D.Q. Li, A statistical quality monitoring method for plastic injection molding using machine built-in sensors, Int. J. Adv. Manuf. Technol. 85 (9–12) (2016) 2483–2494, https://doi.org/10.1007/s00170-015-8013-2.

[11] M.S. Huang, T.Y. Lin, R.F. Fung, Key design parameters and optimal design of a five-point double-toggle clamping mechanism, Appl. Math. Model. 35 (9) (2011) 4304–4320, https://doi.org/10.1016/j.apm.2011.03.001.

[12] R.X. Gao, D.O. Kazmer, Multivariate sensing and wireless data communication for process monitoring in RF-shielded environment, CIRP Ann.-Manuf. Technol. 61 (1) (2012) 523–526, https://doi.org/10.1016/j.cirp.2012.03.014.

[13] F. Lionetto, A. Maffezzoli, Polymer characterization by ultrasonic wave propagation, Adv. Polym. Tech. 27 (2) (2008) 63–73 10.1002.adv.20124.

[14] B.B. He, X. Yuan, H. Yang, H. Tan, L.X. Qian, Q. Zhang, Q. Fu, Ultrasonic measurement of orientation in HDPE/iPP blends obtained by dynamic packing injection molding, Polymer 47 (7) (2006) 2448–2454, https://doi.org/10.1016/j.polymer.2006.02.020.

[15] N. Samet, P. Maréchal, H. Duflo, Ultrasonic characterization of a fluid layer using a broadband transducer, Ultrasonics 52 (3) (2012) 427–434, https://doi.org/10.1016/j.ultras.2011.10.004.

[16] Yusuf U. Okan, Theoretical and experimental investigation of fluid rheology effects on modulated ultrasound propagation, Ultrasonics 54 (7) (2014) 2034–2041, https://doi.org/10.1016/j.ultras. 2014.05.014.

[17] N. Xia, P. Zhao, Y. Zhao, J.F. Zhang, J.Z. Fu, Integrated measurement of ultrasonic parameters for polymeric materials via full spectrum analysis, Polym. Test. 70 (2018) 426–433, https://doi.org/10.1016/j.polymertesting.2018.08.003.

[18] N. Xia, P. Zhao, T.Q. Kuang, Y. Zhao, J.F. Zhang, J.Z. Fu, Nondestructive measurement of layer thickness in water-assisted coinjection-molded product by ultrasonic technology, J. Appl. Polym. Sci. 135 (2018) 46540, https://doi.org/10.1002/app.46540.

[19] A. Wan, L.B. Song, J. Xu, S.L. Liu, K. Chen, Calibration and compensation of machine tool volumetric error using a laser tracker, Int. J. Mach. Tools Manuf 124 (2018) 126–133, https://doi.org/10.1016/j.ijmachtools.2017.10.004.

[20] G.V. Pashkova, A.G. Revenko, A review of application of total reflection X-ray fluorescence spectrometry to water analysis, Appl. Spectrosc. Rev. 50 (6) (2015) 443–472, https://doi.org/10.1080/05704928.2015.1010205.

[21] J.X. Chen, S.W. Lin, X.L. Zhou, A comprehensive error analysis method for the geometric error of multi-axis machine tool, Int. J. Mach. Tools Manuf. 106 (2016) 56–66, https://doi.org/10.1016/j.ijmachtools.2016.04.001.

[22] J. Xie, P. Zhao, C.Q. Zhang, J.Z. Fu, Measuring densities of polymers by magneto-archimedes levitation, Polym. Test. 56 (2016) 308–313, https://doi.org/10.1016/j.polymertesting.2016.10.032.

[23] N. Xia, P. Zhao, J. Xie, C.Q. Zhang, J.Z. Fu, Density measurement for polymers by magneto-Archimedes levitation: simulation and experiments, Polym. Test. 63 (2017) 455–461, https://doi.org/10.1016/j.polymertesting.2017.09.014.

[24] C.Q. Zhang, P. Zhao, F. Gu, J. Xie, N. Xia, Y. He, J.Z. Fu, Single-ring magnetic levitation configuration for object manipulation and density-based measurement, Anal. Chem. 90 (2018) 9226–9233, https://doi.org/10.1021/acs.analchem.8b01724.

[25] J. Xie, P. Zhao, Z.B.Y. Jing, C.Q. Zhang, N. Xia, J.Z. Fu, Research on the sensitivity of magnetic levitation (Maglev) devices, J. Magn. Magn. Mater. 468 (2018) 100–104, https://doi.org/10.1016/j.jmmm.2018.07.082.

[26] N. Xia, P. Zhao, J. Xie, C.Q. Zhang, J.Z. Fu, Non-destructive measurement of three-dimensional polymeric parts by magneto-Archimedes levitation, Polym. Test. 66 (2018) 32–40, https://doi.org/10.1016/j.polymertesting.2018.01.004.

[27] C.Q. Zhang, P. Zhao, J. Xie, N. Xia, J.Z. Fu, Enlarging density measurement range for polymers by horizontal magneto-Archimedes levitation, Polym. Test. 67 (2018) 177–182, https://doi.org/10.1016/j.polymertesting.2018.03.008.

[28] C.Q. Zhang, P. Zhao, W. Wen, J. Xie, N. Xia, J.Z. Fu, Density measurement via magnetic levitation: Linear relationship investigation, Polym. Test. 70 (2018) 520–525, https://doi.org/10.1016/j.polymertesting.2018.08.010.

[29] P. Zhao, J.Z. Fu, S.B. Cui, Non-destructive characterisation of polymers during injection moulding with ultrasonic attenuation measurement, Mater. Res. Innovations 15 (2011) S311–S314, https://doi.org/10.1179/143307511X12858957674355.
[30] W. Michaeli, C. Starke, Ultrasonic investigations of the thermoplastics injection moulding process, Polym. Test. 24 (2) (2005) 205–209, https://doi.org/10.1016/j.polymertesting.2004.08.009.
[31] Y. Ono, B.R. Whiteside, E.C. Brown, M. Kobayashi, C.C. Cheng, C.K. Jen, P.D. Coates, Real-time process monitoring of micromoulding using integrated ultrasonic sensors, Trans. Inst. Meas. Control 29 (5) (2007) 383–401, https://doi.org/10.1177/0142331207080153.
[32] C.C. Cheng, Y. Ono, C.K. Jen, Real-time diagnosis of co-injection molding using ultrasound, Polym. Eng. Sci. 47 (9) (2007) 1491–1500, https://doi.org/10.1002/pen.20852.
[33] L. Mulvaney-Johnson, C.C. Cheng, Y. Ono, E.C. Brown, C.K. Jen, P.D. Coates, Real time diagnostics of gas/water assisted injection moulding using integrated ultrasonic sensors, Plast. Rubb. Compos. 36 (3) (2007) 111–121, https://doi.org/10.1179/174328907X177617.
[34] P. Zhao, S. Wang, J. Ying, J.Z. Fu, Non-destructive measurement of cavity pressure during injection molding process based on ultrasonic technology and Gaussian process, Polym. Test. 32 (8) (2013) 1436–1444, https://doi.org/10.1016/j.polymertesting.2013.09.006.
[35] P. Zhao, Y.Y. Peng, W.M. Yang, J.Z. Fu, L.S. Turng, Crystallization measurements via ultrasonic velocity: study of poly(lactic acid) parts, J. Polym. Sci. Part B-Polym. Phys. 53 (10) (2015) 700–708, https://doi.org/10.1002/polb.23691.
[36] K.Y. Jhang, H.H. Quan, J. Ha, Estimation of clamping force in high-tension bolts through ultrasonic velocity measurement, Ultrasonics 44 (8) (2006) e1339–e1342, https://doi.org/10.1016/j.ultras. 2006.05.190.
[37] L.B. Qi, Y. Wu, M.S. Zou, Y. Duan, M.X. Shen, Acoustic and vibrational characteristics of a propeller-shaft-hull coupled system based on sono-elasticity theory, J. Vib. Control 24 (9) (2018) 1707–1715, https://doi.org/10.1177/1077546316668061.
[38] N.H. Nelson, Acoustical birefringence and the use of ultrasonic waves for experimental stress analysis, Exp. Mech. 14 (5) (1974) 169–176, https://doi.org/10.1007/BF02323061.
[39] C.M. Sayers, Ultrasonic velocities in anisotropic polycrystalline aggregates, J. Phys. D Appl. Phys. 15 (11) (1982) 2157–2167, https://doi.org/10.1088/0022-3727/15/11/011.